The progenitor of the big bang and its connection to the flatness and acceleration of the universe

*Hujeirat A.A.

IWR, Universität Heidelberg, 69120 Heidelberg, Germany

September 5, 2022

Abstract

It was argued that old and massive neutron stars end up as black objects that are made of purely incompressible superconducting gluon-quark superfluid matter (henceforth SuSu-objects). Based on theoretical investigations and numerical solving of the field equations with time-dependent spacetime topologies, I argue that a dense cluster of SuSu-objects at the background of flat spacetime that merged smoothly is a reliable candidate for the progenitor of the big bang. Here we present and use a new time-dependent spacetime metric, which unifies the metrics of Minkowski, Schwarzschild, and Friedmann as well as a modified TOV-equation for modeling dynamical contractions of relativistic objects. Had the progenitor undergone an abrupt decay, a hadronizing front forms at its surface and starts propagating from outside-to-inside, thereby hadronizing its entire content and changing the topology of the embedding spacetime from a flat into a dynamically expanding curved one. For an observer located at the center of the progenitor, $\mathcal{H}_0$, the universe would be seen as isotropic and homogeneous, implying therefore that the last big bang event must have occurred in our neighborhood.

For $t \gg \tau_{dyn}$ the curved spacetime re-converge into a flat one, whereas the outward-propagation topological front, which separates the enclosed curved spacetime from the exterior flat one, would appear spatially and temporally accelerating outwards.

The here-presented scenario suggests possible solutions to the flatness problem, the origin of acceleration of the universe and the pronounced activities of high redshift QSOs .

We anticipate that future observations by the James-Webb-Telescope to support our scenario when active QSOs with $z > 12$ would be detected.

Keywords: General Relativity: big bang, black holes, QSOs, neutron stars, QCD, condensed matter, superfluidity

*E-mail:AHujeirat@uni-hd.de

1 Introduction

Data from supernovae statistics predict that at least 1% of star populations in star-forming clouds should be neutron stars (NSs). Yet this rate is expected to be even higher in the early universe when the first generation of stars was formed, roughly 500 Myr after the big bang (henceforth BB). These should have been massive, extraordinary luminous and therefore short-living, which subsequently collapsed to form BHs or massive NSs [1, 2]. However, their relatively large sizes, masses and energy contents would give rise to fragmentation, preferably forming massive NSs rather than BHs. This may reasonably explain why the mass-function of BHs exhibits the mass-gap: $[2.5M_\odot \leq \mathcal{M} \leq 5.5M_\odot]$, where stellar BHs have not been detected.

Indeed, for the currently measured average density and dimensions, we expect the universe to inhibit 10^{20} NSs [3, 4]. The actual number of NSs may turn out to be much larger, as the universe prior to the BB might have been populated with old objects and inactive galaxies. This is in line with recent observations that reveal the existence of certain stellar components and QSOs formed earlier than the redshift $z \geq 10$ (see [2] and the references therein), i.e. within only several hundred million years after the BB. Also, formation of the high redshift galaxy GN-z11 within 600 Myr after the BB and the possibility that it may host a SMBH cannot be explained by the current evolutionary scenarios [5, 6]. Therefore, NSs may significantly affect the dynamics of the universe on time scales longer than or even comparable to the
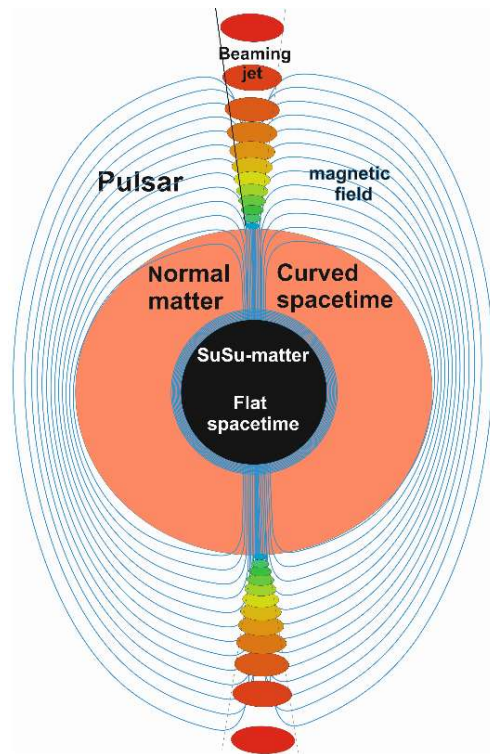

Figure 1: A pulsars with an embryonic quantum core and different spacetime topologies.

age of the universe (henceforth τ_{14}.)

On $\tau \geq \tau_{14}$, NSs have ample time to conglomerate into clusters and subsequently merge to form progenitors to numerous BB-events that take off sequentially and in parallel.

But what is the nature of NS-cores? Most theoretical and numerical studies of NS-interiors predict the central density to be larger than the nuclear density, ρ_0. Due to the vanishing thermal energy production inside the core, the average gradient of the temperature throughout the NS should be positive, and therefore the core is practically a "freezer" of zero-temperature. Under these conditions, supranuclear dense matter has little choice, but to be superfluid. These arguments are in line with well-observed

glitch phenomena in pulsars (see [7, 8, 9, 10] for further details).

Superconductivity ensures that magnetic fields are expelled from the zero-temperature core into the boundary layer between the core and the overlaying compressible and dissipative normal matter. Based on our previous studies (e.g. [10]) the spacetime embedding the SuSu-core should be flat, whereas the overlaying normal matter is embedded in a curved spacetime (Fig. 1).

In fact the over- and undershooting that have been observed to associate the glitching events of the Vela pulsar in 2016 provide further evidence for the conductivity and superfluidity of the cores in massive NSs [11, 12]. The overall configuration is strikingly similar to the tachocline between the convection zone of the sun and the underlying rigid body rotating core, where dynamo action is considered to be operating.

Demanding the core's matter to be purely incompressible is a very strong requirement with far-reaching consequences in astrophysics and cosmology. To clarify the point, a fluid is said to be incompressible, if the density-gradient vanishes everywhere in the domain, i.e. $\nabla \mathcal{E} = 0$. In terrestrial incompressible fluids, the pressure ceases to describe the thermodynamical state of matter locally, but it turns into a mathematical term only, called the lagrangian multiplier, which affects the dynamical behavior of the fluid globally, irrespective of causality.

In stars, incompressibility is a requirement that is fulfilled through the imposed regularity condition at the center of astrophysical objects. In the case of NSs, the pressure gradient ∇P is generally balanced by the spatial variation of the curvature $\nabla_\mu g^{\mu\nu}$, which is dominated by $\nabla_\mu g^{\mu\nu} \approx \Delta g_{tt}/\Delta r$. On length scales comparable to the average separation between two arbitrary nucleons Δr_{bb}, the relative spatial variation of $|g_{\mu\nu}|$ is of order 10^{-19} [13], and therefore too weak compared to the governing nuclear forces.

On the other hand, the cores of old and massive NSs are made of zero-temperature supranuclear dense matter. Under these conditions, it was conjectured that the matter must be made of an incompressible superconducting gluon-quark superfluid [14]. While superconductivity and superfluidity are direct consequences of zero-temperature dense matter even under terrestrial conditions, the incompressibility of gluon-quark matter would remain a hypothesis that may not be verified under normal conditions. However, there is a reasonable argument in favor of the incompressibility of gluon-quark matter at zero-temperature: Given that gluon-quark-plasmas inside hadrons are hidden from the outside world, this may indicate that the energy states of QGP inside hadrons are incompatible with the surrounding particle-free vacuum structure [15, 16]. At zero-temperature however, a QGP is expected to undergo a phase transition into QG-condensate, where QG settles down into the lowest possible quantum energy state predicted to be compatible with that of the surrounding particle-free vacuum. In this case, putting a certain number of QG-condensates together, the vacuum would share the same energy states. Here the QG-condensates become transparent to each other, and so they merge to form a parent

QG-condensate, whose size is the linear addition of the individuals.

As the spacetime embedding vacuum is flat, then the spacetime embedding the parent zero-temperature QG-condensate should be flat too, which is equivalent to requiring the QG-cloud to be macroscopically incompressible. In fact, recent results from the Relativistic Heavy Ion Collider (RHIC) confirm that the quark-gluon-plasmas emerging from smashed nuclei behave nearly as perfect liquids [17, 18], though the physical conditions governing the QGP here are totally different from those inside the cores of massive NSs.

Based thereon, the scenario here may be extended to suggest an alternative model for BB without invoking inflation to solve the horizon and flatness problems, as well as prohibit the progenitor from collapsing into a hypermassive BH (see [19, 20, 21] and [22] for a review). Using recent WIMP observations, the total mass content of normal matter in the universe can be calculated and, when divided by the universal maximum energy-density ρ_{cr}^{uni} (≈ 3 ρ_0 see [14] for further details), then a radius of several AUs may be obtained. Prior to the BB-explosion, the progenitor, which was entirely made of incompressible SuSu-matter, was levitating freely in a flat spacetime.

Any model of the BB should still fulfill the classical conditions of isotropy and homogeneity [23]. However, according to our scenario, the progenitor must have a finite measurable size and a certain location in spacetime. These conditions may safely be met for observers located at the center of the progenitor, which implies that the BB of our universe must have occurred in our close neighborhood. Of course, this would violate the cosmological principle grossly, but the model should be taken seriously as long as its implications agree with observations.

2 Theory of the time-dependent spacetime topology of the fireball

Our model is based on the hypothesis that the spacetime embedding incompressible SuSu-matter is flat, and that the progenitor of the BB is a hypermassive DEO that formed from the merger of trillions of stellar mass DEOs on time scales comparable to or longer than the age of the universe.

Hence, $t \leq 0$ relative to $\mathcal{H}_0$ the spacetime both inside and outside the progenitor was Minkowski flat, i.e. $ds^2_{Mink} = \eta_{\mu\nu}dx^\mu dx^\nu$. However, at $t = 0^+$, the confining force at the surface of the progenitor suffered an irreversible destructive decay, which triggered a hadronization front that propagated from outside-to-inside, thereby converting the rings of SuSu-matter into a dissipative and compressible matter successively, which is dubbed normal matter. This matter interacts with the embedding spacetime and dictates its curvature. In the stationary case, Birkhoff theorem states that the spacetime surrounding the newly formed rings of normal matter should be of the Schwarzschild-type metric, $ds^2_{Sch} = g_{\mu\nu}dx^\mu dx^\nu$.

If the metric is time-dependent, then the transitions

from ds^2_{Mink} into ds^2_{Sch} or even into the Friedmann-Robertson-Wakker metric (FRW), ds^2_{FRW}, and vice versa, should be possible, depending on the amount and type of the embedded matter .

Let ds^2 be a metric, which has the following form:

$$
\begin{aligned}
ds^2 &= g_{\mu\nu}dx^\mu dx^\nu \\
&= g_{00}\,dt^2 + g_{11}\,d\bar{r}^2 + g_{22}\,d\theta^2 + g_{33}\,d\varphi^2
\end{aligned}
\tag{1}
$$

where

$$
\begin{aligned}
g_{00} &= c^2\,e^{2\mathcal{V}(r,t)}, \quad g_{11} = -e^{2\lambda(r,t)} \\
g_{22} &= -e^{2\mathcal{C}(t)}r^2, \quad g_{33} = -e^{2\mathcal{C}(t)}r^2 sin^2\theta.
\end{aligned}
\tag{2}
$$

Here $\mathcal{V}$, and λ are functions of the comoving radius $\bar{r}(r,t) = r\,e^{\mathcal{C}}$, and $\mathcal{C}(t)$ is a function of time only. All physical and geometrical events are measured with respect to $\mathcal{H}_0$ located at $r = 0$.

When contracting the Riemann tensor and calculating the Ricci tensor (see [23] for further details):

$$
R_{\mu\nu} = \Gamma^\alpha_{\mu\alpha,\nu} - \Gamma^\alpha_{\mu\nu,\alpha} + \Gamma^\alpha_{\mu\beta}\Gamma^\beta_{\alpha\nu} - \Gamma^\alpha_{\mu\nu}\Gamma^\beta_{\alpha\beta},
\tag{3}
$$

using the Christoffel symbol:

$$
\Gamma^\lambda_{\mu\nu} = \frac{1}{2}g^{\lambda\kappa}\{g_{\kappa\nu,\mu} + g_{\kappa\mu,\nu} - g_{\mu\nu,\kappa}\},
\tag{4}
$$

we obtain the following Ricci components:

$$
\begin{aligned}
R_{00} &= \ddot{\lambda} + \dot{\lambda}^2 - \dot{\mathcal{V}}\dot{\lambda} + 2\ddot{\mathcal{C}} + 2\dot{\mathcal{C}}^2 - 2\dot{\mathcal{V}}/r \\
&+ (-\mathcal{V}'' + \mathcal{V}'\lambda' - (\mathcal{V}')^2 - 2\mathcal{V}'/r)\,e^{2(\mathcal{V}-\lambda)} \\
R_{11} &= (-\ddot{\lambda} - \dot{\lambda}^2 + \dot{\mathcal{V}}\dot{\lambda} - 2\dot{\lambda}\dot{\mathcal{C}})\,e^{2(\lambda-\mathcal{V})} \\
&+ \mathcal{V}'' + (\mathcal{V}')^2 - \mathcal{V}'\lambda' - 2\lambda'/r \\
R_{22} &= -\{\ddot{\mathcal{C}} + \dot{\mathcal{C}}\dot{\lambda} + 2\dot{\mathcal{C}}^2 - \dot{\mathcal{V}}\dot{\mathcal{C}}\}r^2\,e^{2(\mathcal{C}-\mathcal{V})} \\
&+ (1 + r\mathcal{V}' - r\lambda')\,e^{2(\mathcal{C}-\lambda)} - 1 \\
R_{33} &= -r^2 sin^2\theta\,[\ddot{\mathcal{C}} + 2\dot{\mathcal{C}}^2 - \dot{\mathcal{V}}\dot{\mathcal{C}} + \dot{\mathcal{C}}\dot{\lambda}]\,e^{2(\mathcal{C}-\mathcal{V})} \\
&+ sin^2\theta\,[(1 + r\mathcal{V}' - r\lambda')\,e^{2(\mathcal{C}-\lambda)} - 1].
\end{aligned}
\tag{5}
$$

$\dot{\Box}, \Box'$ denote the time and spatial-derivatives of the variables, respectively.

The field equations may be re-arranged into the convenient form:

$$
\begin{aligned}
R^{(t)}_{00} + R^{(s)}_{00}\,e^{2(\mathcal{V}-\lambda)} &= RHS_{00} \\
R^{(t)}_{11}\,e^{2(\lambda-\mathcal{V})} + R^{(s)}_{11} &= RHS_{11} \\
R^{(t)}_{22}\,r^2\,e^{2(\mathcal{C}-\mathcal{V})} & \\
+ R^{(s)}_{22}\,e^{2(\mathcal{C}-\lambda)} - 1 &= RHS_{22},
\end{aligned}
\tag{6}
$$

where

$$
\begin{aligned}
R^{(t)}_{00} &= \ddot{\lambda} + \dot{\lambda}^2 - \dot{\mathcal{V}}\dot{\lambda} + 2\ddot{\mathcal{C}} + 2\dot{\mathcal{C}}^2 - 2\dot{\mathcal{V}}/r \\
R^{(t)}_{11} &= -\ddot{\lambda} - \dot{\lambda}^2 + \dot{\mathcal{V}}\dot{\lambda} - 2\dot{\mathcal{C}}\lambda \\
R^{(t)}_{22} &= -(\ddot{\mathcal{C}} + 2\dot{\mathcal{C}}^2 - \dot{\mathcal{C}}\dot{\mathcal{V}} + \dot{\mathcal{C}}\dot{\lambda})
\end{aligned}
$$

and

$$
\begin{aligned}
R^{(s)}_{00} &= (-\mathcal{V}'' + \mathcal{V}'\lambda' - (\mathcal{V}')^2 - 2\mathcal{V}'/r) \\
R^{(s)}_{11} &= \mathcal{V}'' + (\mathcal{V}')^2 - \mathcal{V}'\lambda' - 2\lambda'/r \\
R^{(s)}_{22} &= 1 + r\mathcal{V}' - r\lambda'.
\end{aligned}
\tag{7}
$$

To make the problem tractable, the field equations:

$$
\mathcal{R}_{\mu\nu} - \frac{1}{2}g_{\mu\nu}\mathcal{R} + \Lambda g_{\mu\nu} = -\kappa\mathcal{T}_{\mu\nu},
\tag{8}
$$

may be re-written in the following equivalent form:

$$
\mathcal{R}_{\mu\nu} = -\kappa(\mathcal{T}_{\mu\nu} - \frac{T}{2}g_{\mu\nu}) + \Lambda g_{\mu\nu} = RHS_{\mu\nu},
\tag{9}
$$

where $\mathcal{T} = \mathcal{T}^\mu_\mu$, $\mathcal{T}_{\mu\nu}$ and Λ correspond to the stress-energy tensor and the cosmological constant, respectively (see [13, 23] for further details).

Expanding the tensor $RHS_{\mu\nu}$ we obtain:

$$
\begin{aligned}
RHS_{\mu\nu} &= -\kappa(T_{\mu\nu} - \frac{T}{2}g_{\mu\nu}) + \Lambda g_{\mu\nu} \\
&= -\kappa g_{\mu\nu}[(\rho+p)u_\mu u^\nu - \frac{1}{2}(\rho-p)] + \Lambda g_{\mu\nu} \\
&= \{-\kappa[(\rho+p)u_\mu u^\nu - \frac{1}{2}(\rho-p)] + \Lambda\}g_{\mu\nu}
\end{aligned}
\tag{10}
$$

5

The diagonal components have the following forms:

$$
\begin{aligned}
RHS_{00} &= \{-\kappa[(\rho+p)\Gamma^2 g_{00} - \tfrac{1}{2}(\rho-p)] + \Lambda\}g_{00} \\
&= \overline{RHS}_{00}\, g_{00} \\
RHS_{11} &= \{-\kappa[(\rho+p)\Gamma^2 V^2\, g_{11} - \tfrac{1}{2}(\rho-p)] + \Lambda\}\, g_{11} \\
&= \overline{RHS}_{11}\, g_{11} \\
RHS_{22} &= \{\tfrac{\kappa}{2}[(\rho-p)] + \Lambda\}g_{22}, \\
&= \overline{RHS}_{22}\, g_{22}.
\end{aligned}
\tag{11}
$$

Here $\Gamma = 1/\sqrt{(g_{00} + g_{11}V^2)}$ and V are the Lorenz factor and the transport velocity as measured by $\mathcal{O}_0$, respectively.

The above set of equations may be re-written in a more convenient form:

$$
\begin{aligned}
R_{00}^{(t)}\, e^{-2\mathcal{V}} + R_{00}^{(s)}\, e^{-2\lambda} &= \overline{RHS}_{00} \\
R_{11}^{(t)}\, e^{-2\mathcal{V}} + R_{11}^{(s)}\, e^{-2\lambda} &= -\overline{RHS}_{11} \\
R_{22}^{(t)}\, e^{-2\mathcal{V}} + \tfrac{R_{22}^{(s)}}{r^2}\, e^{-2\lambda} - \tfrac{e^{-2\mathcal{C}}}{r^2} &= -\overline{RHS}_{22}.
\end{aligned}
\tag{12}
$$

Subtracting the second equation from the first in (12), and dividing by 2, yields:

$$
\begin{aligned}
\tfrac{1}{2}\left(R_{00}^{(t)} + R_{11}^{(t)}\right) e^{-2\mathcal{V}} &- \left(\tfrac{\mathcal{V}'+\lambda'}{r}\right) e^{-2\lambda} \\
&= -\tfrac{1}{2}\kappa[(\mathcal{E}+p)\Gamma^2(g_{00} - g_{11}V^2)].
\end{aligned}
\tag{13}
$$

Now, adding the last equation to the third, we obtain:

$$
\begin{aligned}
[\tfrac{1}{2}\left(R_{00}^{(t)} + R_{11}^{(t)}\right) + R_{22}^{(t)}]\, e^{-2\mathcal{V}} &- \tfrac{1}{r^2}\tfrac{d}{dr}(r(e^{-2\mathcal{C}} - e^{-2\lambda}) \\
= -\tfrac{1}{2}\kappa[(\mathcal{E}+p)\Gamma^2(g_{00} &- g_{11}V^2) + (\rho-p)] - \Lambda,
\end{aligned}
\tag{14}
$$

where,

$$
\begin{aligned}
\tfrac{1}{2}(R_{00}^{(t)} + R_{11}^{(t)}) &= \ddot{\mathcal{C}} + \dot{\mathcal{C}}^2 - \dot{\lambda}\dot{\mathcal{C}} - \tfrac{\ddot{\mathcal{V}}}{r} \\
\tfrac{1}{2}(R_{00}^{(s)} + R_{11}^{(s)}) &= -\tfrac{\mathcal{V}'+\lambda'}{r} \\
\tfrac{1}{2}\left(R_{00}^{(t)} + R_{11}^{(t)}\right) + R_{22}^{(t)} &= -\dot{\mathcal{C}}^2 + (\dot{\mathcal{V}} - 2\dot{\lambda})\dot{\mathcal{C}} - \tfrac{\ddot{\mathcal{V}}}{r} \\
\tfrac{1}{2}\left(R_{00}^{(s)} + R_{11}^{(s)}\right) + R_{22}^{(s)} &= -\tfrac{1}{r^2}\tfrac{d}{dr}(r(e^{-2\mathcal{C}} - e^{-2\lambda}).
\end{aligned}
\tag{15}
$$

As the last equation in (14) must be applicable both to stationary and time-dependent cases, then $e^{-2\lambda} = e^{-2\mathcal{C}} \times f(r,t)$. However, in the stationary case, Birkhoff theorem states that outside the object, $f(r,t) \sim 1/(1 - \mathcal{X}(r))$. Therefore, without loss of generality, we may set the metric components to be of the forms:

$$
g_{11} = -e^{2\lambda} = \tfrac{e^{2C}}{1-\mathcal{X}_b}, \quad \text{and} \quad e^{2C} = R^2,
\tag{16}
$$

where $R = R(t)$ and $\mathcal{X}_b = \mathcal{X}_b(r,t)$. The subscript "b" corresponds to the function in the comoving frame. Further inspection of the equations (see Eq. 20), shows that, for a slowly varying $\mathcal{V}$ and $V \ll c$, we obtain:

$$
\frac{1}{r^2 R^2}\frac{d}{dr}(r\mathcal{X}_b)) \sim \kappa\mathcal{E},
$$

whose integration yields $\mathcal{X} \sim m/r$, where $m = 4\pi \int \mathcal{E}r^2 dr$ is the enclosed mass. It turns out that setting $\mathcal{X}_b(r,t) = m_b(r,t)/r$ provides consistent solutions for almost all reasonable metrics. In this case, the derivatives of $\mathcal{V}$ read as follows:

$$
\lambda' = \tfrac{1}{2}\frac{\mathcal{X}_b'}{1-\mathcal{X}_b},
$$

$$
\dot{\lambda} = \begin{cases} \dot{\mathcal{C}} & ; \text{ if } \dot{\mathcal{X}}_b = 0, \\ \dot{\mathcal{C}} + \tfrac{1}{2}\frac{\dot{\mathcal{X}}_b}{(1-\mathcal{X}_b)} \\ = (1 + \mathcal{Z}_b)\dot{\mathcal{C}} + \dot{F} & ; \text{ otherwise} \end{cases}
\tag{17}
$$

where $\dot{\mathcal{C}} = \dot{R}/R$, $\mathcal{Z}_b = \mathcal{X}_b/(1 - \mathcal{X}_b)$ and $\dot{F}$ is a material flux function of the form:

$$
\dot{F} = \frac{1}{2}\frac{\alpha_{bb}}{r}\frac{\dot{m}_b^{nor}}{(1 - \mathcal{X}_b)}.
\tag{18}
$$

Hence the set of field equations that describes the time-evolution of the spacetime topology reads:

$$
\begin{aligned}
&[\tfrac{\ddot{R}}{R} - (1 + \mathcal{Z}_b)\left(\tfrac{\dot{R}}{R}\right)^2 - \dot{F}\left(\tfrac{\dot{R}}{R}\right)]\, e^{-2\mathcal{V}} \\
&+ \tfrac{1}{2r}[\tfrac{\partial}{\partial t}(e^{-2\mathcal{V}}) + \tfrac{e^{-2\lambda}}{e^{-2\mathcal{V}}}\tfrac{\partial}{\partial r}(e^{-2\mathcal{V}}) + \tfrac{\partial}{\partial r}e^{-2\lambda}] \\
&= -\tfrac{1}{2}\kappa(\mathcal{E}+p)[\Gamma^2(g_{00} - g_{11}V^2)]
\end{aligned}
\tag{19}
$$

6

$$\frac{1}{2}\left(\frac{1}{r}-Y\right)\frac{\partial}{\partial t}(e^{-2\mathcal{V}})$$
$$-[(3+2\,\mathcal{Z}_b)\left(\frac{\dot{R}}{R}\right)^2+2\,\dot{F}\left(\frac{\dot{R}}{R}\right)]e^{-2\mathcal{V}}$$
$$=-\kappa(\mathcal{E}+p)\,V^2 e^{-2(\mathcal{V}-\lambda)} \qquad (20)$$
$$+\frac{1}{r^2 R^2}\frac{d}{dr}(r\mathcal{X}_b))-\kappa\mathcal{E}.$$

In addition, the conservation of energy and momentum of matter is taken into account by requiring that the the stress-energy tensor must be divergence-free, i.e. $\nabla_\mu T^{\mu\nu}=0$. This yields the following set of GR hydrodynamical equations:

$$\frac{1}{\sqrt{-g}}\frac{\partial}{\partial t}(\sqrt{-g}\mathcal{D})+\frac{1}{R}\frac{1}{\sqrt{-g}}\frac{\partial}{\partial r}\sqrt{-g}(\mathcal{D}V)=0 \quad (21)$$

$$\frac{1}{\sqrt{-g}}\frac{\partial}{\partial t}(\sqrt{-g}\mathcal{M}^r)+\frac{1}{R}\frac{1}{\sqrt{-g}}\frac{\partial}{\partial r}(\sqrt{-g}\mathcal{M}^r V)$$

$$=-\frac{1}{R}\frac{\partial P}{\partial r}+\frac{\mathcal{M}^t}{2R}(g_{tt,r}+V^2 g_{rr,r}), \qquad (22)$$

where $\sqrt{-g}=r^2 R^3\sin(\theta)/\sqrt{GW}$, $\mathcal{D}$, and V are the determinant of the metric, the relativistic energy-density, and the transport velocity, respectively. The four-momenta is defined as $\mathcal{M}^\sigma=\mathcal{D}hu^\sigma$, where h stands for enthalpy and u^σ for the four-velocity; $\sigma=\{t,r,\theta,\varphi\}$. Here, the Lorentz factor reads:

$$u^t=\frac{1}{g_{tt}+V^2 g_{rr}}. \qquad (23)$$

The continuity equation may be re-written in the following compact form:

$$\frac{\partial}{\partial t}(\overline{\mathcal{D}}_b)+\frac{1}{R}\frac{1}{r^2}\frac{\partial}{\partial r}(r^2\overline{\mathcal{D}}_b V)=0, \qquad (24)$$

where $\overline{\mathcal{D}}_b=\mathcal{D}_b/\sqrt{GW}$ and $\mathcal{D}_b=\mathcal{D}R^3$. To close the system, an equation of state (EOS) should be included, e.g. $P=P(\mathcal{E})=P(\mathcal{D}/u^t)$.

2.1 Special cases

In the above-mentioned derivations both the metric coefficients g_{tt} and g_{rr} are spatially and temporally varying functions. The simplest special case is Minkowski spacetime, where $g_{tt}\to 1$ and $g_{tt}\to -1$. The Schwarzschild metric may be recovered by relaxing the time-dependency, setting $R=1$, $V=0$ and $\mathcal{X}=\frac{2G}{c^2}\frac{m(r)}{r}$, where $m(r)$ denotes the enclosed mass of normal matter. The FRW metric is recovered by setting both the energy density and the metric coefficient g_{tt} to constants.

However, it is tempting to see how the above set of equations yields the TOV equation in the case of an object in hydrostatic equilibrium, embedded in a Schwarzschild spacetime as well as the Friedmann equations in the case of an expanding universe.

2.1.1 The modified TOV equation for modeling slowly contracting relativistic objects

Assume we are given a non-rotating and demagnetized relativistic object of normal matter with a constant energy-density. Following Birkhoff theorem, the surrounding spacetime topology may be described by the Schwarzschild metric. Depending on the EOS, the object may undergo a dynamical collapse or contract slowly, where in both cases the matter is transported from outside-to-inside with the transport velocity $V\ll c$. Similar to other stationary observers, our preferred central observer, O_0 may measure the contraction of the object with $R(t)=1$.

In this case, Eq.(19) reduces to:

$$\left[\frac{1}{2r}\left[\frac{\partial}{\partial t}(e^{-2\mathcal{V}}) + \frac{e^{-2\lambda}}{e^{-2\mathcal{V}}}\frac{\partial}{\partial r}(e^{-2\mathcal{V}}) + \frac{\partial}{\partial r}e^{-2\lambda}\right]\right.$$
$$= -\frac{1}{2}\kappa(\mathcal{E}+p)[\Gamma^2(g_{00}-V^2 g_{11})] = -\frac{1}{2}\kappa(\mathcal{E}+p)\overline{\overline{\Gamma}}, \tag{25}$$

where $\overline{\overline{\Gamma}}$ is the modified Lorentz factor. Inserting:

$$\frac{\partial e^{-2\lambda}}{\partial r} = \frac{\mathcal{X}'}{R^2} = \frac{\alpha_{bb}}{R}\left(\frac{m_b}{r}\right)' = \frac{\alpha_{bb}}{R}\left(\frac{m_b'}{r} - \frac{m_b}{r^2}\right),$$

where $\alpha_{bb} = \frac{2G}{c^2}$ and re-arranging terms, we end up with the following equation:

$$(e^{-2\lambda})\frac{\partial e^{-2\mathcal{V}}}{\partial t} + \frac{\partial \mathcal{V}}{\partial r} = -3\frac{\alpha_{bb}}{R}\left(\overline{\overline{\Gamma}}^2 - 1\right)\frac{\mathcal{E}_b\, r}{1-\mathcal{X}_b}$$
$$-\frac{\alpha_{bb}}{R}\frac{(m_b + 3r^3 P_b \overline{\overline{\Gamma}}^2)}{r^2\,(1-\mathcal{X}_b)}. \tag{26}$$

Since a small mass perturbation would hardly affect the global topology of spacetime on time scales much shorter than the dynamical time scale, the time-derivative of $\mathcal{V}$ may be replaced by a numerical smoother, which enables the $\mathcal{V}-$integration throughout the whole domain, where the conditions at the outer boundary are used.

Note that when the transport velocity vanishes, the modified Lorentz factor reduces to one, i.e., $\overline{\overline{\Gamma}}^2 = 1$, and the classical TOV equation:

$$\frac{\partial \mathcal{V}}{\partial r} = -\frac{\alpha_{bb}}{R}\frac{(m_b + 3r^3 P_b)}{r^2\,(1-\mathcal{X}_b)}, \tag{27}$$

is then recovered. The effect of the first term on the RHS of Eq. (26) is to steepen the gradient of the energy density in the vicinity of the surface, which yields smaller radii of NSs than usually obtained using the classical TOV equation.

2.1.2   Friedmann Universe

The Friedmann universe may be recovered by setting $V = P = 0$, and $\mathcal{V} = \mathcal{E} =$ constants. In this case, the components of the material tensor on the RHS of Eq. (11) reduce to:

$$\overline{RHS}_{00} = -\frac{\kappa}{2}(\rho + 3\,p) + \Lambda$$
$$\overset{dust}{\longrightarrow} -\frac{\kappa}{2}\rho + \Lambda$$
$$\overline{RHS}_{11} = \frac{\kappa}{2}(\rho - p) + \Lambda \tag{28}$$
$$\longrightarrow \frac{\kappa}{2}\rho + \Lambda$$
$$\overline{RHS}_{22} = \frac{\kappa}{2}(\rho - p) + \Lambda$$
$$\longrightarrow \frac{\kappa}{2}\rho + \Lambda.$$

Setting $\dot{\mathcal{X}} = \mathcal{X}' = 0$ and inserting $\mathcal{X}(r) = k\,r^2$ on the LHS of the Eq.(13), it can be easily verified that the different terms reduce to the following expressions:

$$\frac{1}{2}\left(R_{00}^{(t)} + R_{11}^{(t)}\right)e^{-2\mathcal{V}} \longrightarrow \frac{\ddot{R}}{R} - \left(\frac{\dot{R}}{R}\right)^2$$
$$-\left(\frac{\mathcal{V}'+\lambda'}{r}\right)e^{-2\lambda} \longrightarrow -\frac{k}{R^2} \tag{29}$$
$$-\frac{1}{2}\kappa(\mathcal{E}+p)[1 + 2V^2\frac{W}{G}] \longrightarrow -\frac{1}{2}\kappa\mathcal{E}.$$

Adding these terms together yields the first Friedmann equation:

$$\frac{\ddot{R}}{R} - \left(\frac{\dot{R}}{R}\right)^2 - \frac{k}{R^2} = -\frac{1}{2}\kappa\mathcal{E}. \tag{30}$$

Similarly, Eq. (14) reduces to:

$$\left[\frac{1}{2}\left(R_{00}^{(t)} + R_{11}^{(t)}\right) + R_{22}^{(t)}\right]e^{-2\mathcal{V}} \longrightarrow -3\left(\frac{\dot{R}}{R}\right)^2$$
$$-\frac{1}{r^2}\frac{d}{dr}(r(e^{-2\mathcal{C}} - e^{-2\lambda})) \longrightarrow -3\frac{k}{R^2}$$
$$-\frac{1}{2}\kappa[(\mathcal{E}+p)\Gamma^2(g_{00}-g_{11}V^2)$$
$$+(\rho - p)] + 2\Lambda \longrightarrow -(\kappa\mathcal{E}+\Lambda) \tag{31}$$

Hence, adding these terms together, we obtain:

$$\left(\frac{\dot{R}}{R}\right)^2 = \frac{\kappa}{3}\mathcal{E} + \frac{\Lambda}{3} - \frac{k}{R^2}. \tag{32}$$

Substituting $\left(\frac{\dot{R}}{R}\right)^2$ into Eq. (30), we recover the classical form of Friedmann's first equation:

$$\frac{\ddot{R}}{R} = -\frac{1}{2}\frac{\kappa}{3}\mathcal{E} + \frac{\Lambda}{3}. \tag{33}$$

8

In terms of the classical cosmological parameters Ω_i, the dimensionless scale parameter $a = R/R_0$, and the dimensionless time-variable $\tau = H_0(t - t_0)$, Eq. (30) may be transformed into the following form:

$$\left(\frac{da}{d\tau}\right)^2 = \frac{\Omega_{m,0}}{a} + \frac{\Omega_{r,0}}{a^2} + \Omega_{k,0} + \Omega_{\Lambda,0}\, a^2. \qquad (34)$$

The subscript "0" denotes the value of the corresponding parameter in the present time (see [23] for further details). Depending on the specific values of $\Omega_{i,0}$, the dimensionless scale parameter a may converge or diverge as the system evolves with time.

3 The numerical approach

For solving the set of field equations a new numerical solver has been developed. The solver is unconditionally stable, as it is based on implicit time-integration using preconditioning techniques of Krylov sub-space iterative methods. In the finite space, the equations are discretized using finite volume formulation to ensure mass and energy conservation. In Fig. (2) a schematic description of the solution method is depicted (for further details on the projection method and preconditioning techniques see [24, 25]):
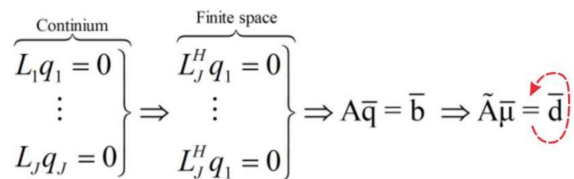

Figure 2: The numerical procedure: the set of analytical equations is transformed into the finite space, $\mathcal{H}$, using the finite volume discretization strategy. The set of equations in $\mathcal{H}$ in operator form read: $L^H q = b^H$, which may be re-written in matrix form as $Aq = b$, where A is the corresponding matrix of coefficients. The matrix equation is then simplified and replaced by $\tilde{A}\mu = d$, where $\tilde{A}$ is a preconditioner that shares the eigenvalues of A, $\overline{\mu}$ is a correction vector that entails deviations from the original solution and d is the defect. The iteration procedure should continue until the maximum norm of $\overline{\mu}$ has dropped below the tolerance value.

4 Time evolution of the fireball: numerical investigation

The form of g_{rr} in both stationary and time-dependent cases, has the following form:

$$g_{rr} = \frac{1}{1 - \mathcal{X}_b}$$
$$\text{where} \qquad (35)$$
$$\mathcal{X}(r,t)_b = \frac{2G}{c^2} R^2 \left(\frac{m(r,t)}{r}\right) = \alpha_{bb}\left(\frac{m_b(r,t)}{rR}\right)$$

$\mathcal{X}(r,t)$ is practically the communicator that tells spacetime how to curve. Let us address the following possibilities for $\mathcal{X}$:
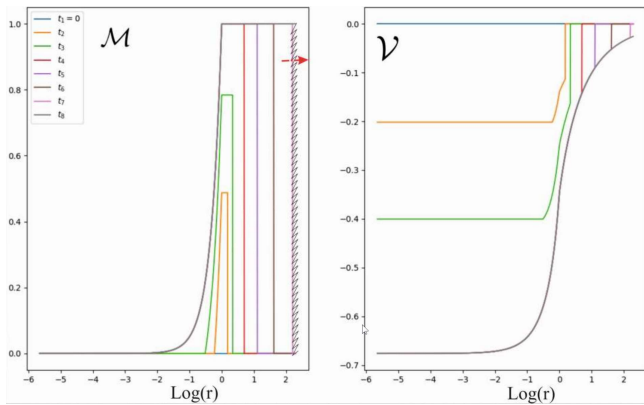
9

Figure 3: Different snapshots of the profile of total mass of normal matter, $\mathcal{M}$, and the gravitational potential $\mathcal{V}$, during the propagations of both the inward-oriented hadronization, $\mathcal{F}^{HA}$, and the outward-oriented expansion front, $\mathcal{F}^{EX}$. In these calculations, hydrodynamics are not included.

$$\mathcal{X}(r,t) \sim \begin{cases} r^2 : & \text{Schwarzschild} \\ & \text{TOM: incompressible normal fluids} \\ r^\alpha : & \text{Schwarzschild} \\ & \text{Normal compressible, } \alpha < 2. \\ r^2 : & \text{Friedmann} \\ & \text{dust} \\ 0 : & \text{Flat} \\ & \text{Vacuum (particle-free spacetime)} \\ 0 : & \text{Flat} \\ & \text{Incompressible SuSu-matter,} \end{cases}$$
(36)

where TOM stands for the "Type Of Matter".

It should be noted here that in the case of incompressible normal matter with $\mathcal{E} = \mathcal{O}(\mathcal{E}_0)$, the field equations lose their predictability power and would enforce the pressure to become ultrabaric and acausal.

The dependence on time endows $\mathcal{X}_b(r,t)$ with an-
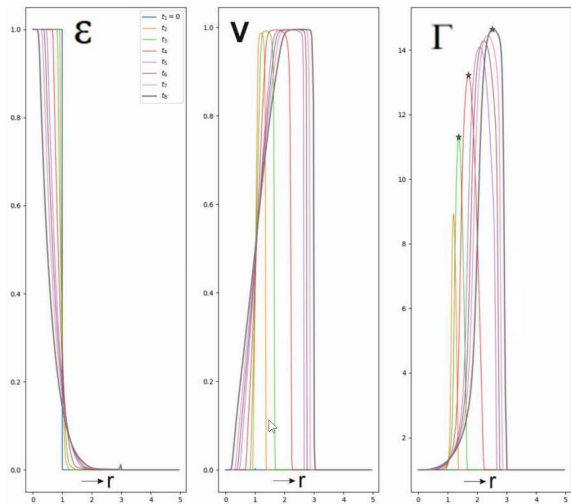
Figure 4: Radial distributions of the energy-density $\mathcal{E}$, transport velocity, V, and Lorentz factor, Γ, at different times are shown. When the quantum surface tension confining the SuSu-matter inside the progenitor is destructively perturbed, a hadronization front forms at the surface which, in turn, generates pressure, whose ∇P sets the newly created normal matter into outward-oriented motion at ultra-high relativistic speeds. The spacetime shortly after the formation of the hadronization front is flat and therefore the flow configuration is identical to the classical relativistic Riemann problem.

Figure 5: Snapshots of the radial distribution of the energy density $\mathcal{E}$, the total mass of normal matter, $\mathcal{M}$, the transport velocity, $\mathbf{V}$, the modified Lorentz factor, $\overline{\overline{\Gamma}}$, and the gravitational potential, $\mathcal{V}$, during contraction of a DEO. The boundary conditions here do not allow transport of normal matter into the surrounding space. In these calculations, an enhanced shock-capturing method is developed to 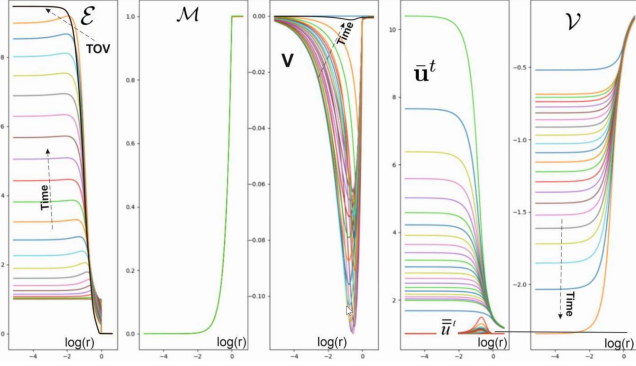avoid bouncing. The final configuration here is shown to converge smoothly into forming a core in hydrostatic equilibrium, whose interior may be well-described by the classical TOV equation.

other degree of freedom: The topology of spacetime depends not only on the total mass, but on the nature of matter also, and in particular, the spacetime should be prepared to immediately change its topology, depending on whether it embeds normal compressible matter, SuSu-matter, or particle-free vacuum.

In the present case, the progenitor of the BB is made of incompressible SuSu-matter. Hence prior to the BB, i.e., for $t \leq 0$ relative to $\mathcal{O}_0$, the embedding spacetime was flat.

However, at $t = 0$ the fine-tuned surface tension confining the enclosed ocean of the SuSu-matter inside the progenitor, undergoes an abrupt decay, through which a hadronizing front is formed, which propa-

gates from outside-to-inside. Behind the front, the deconfined SuSu-matter converts into hadrons. The released energy, which is expected to be of the order of 1 GeV per hadron, creates an extraordinary huge pressure, whose ∇P enforces the newly created normal matter to propagate outwards with ultrarelativistic velocity. This velocity may be predicated from the momentum Equation (22) as follows:

$$\frac{\partial \bar{u}^u}{\partial t} \approx -\frac{\nabla P}{D} + f_{grav} \Rightarrow (\bar{u}^u)^2 \approx \frac{P_u}{D} = V_S^2 \approx c^2, \tag{37}$$

where $\bar{u}^u$ is the radial component of the contravariant four-velocity. We used $\Delta r = \Delta_{bb}$ as the length scale over which ∇P changes significantly.

As it will be explained later, since $|f_{grav}| \xrightarrow[r \to \infty]{} 0$, and therefore its decelerating effect decreases with the distance to $\mathcal{O}_0$, and therefore the outward-moving particles would naturally be seen as accelerating outwards. In particular, the particles in the outermost shells, where the topology hardly differs from that of a flat spacetime.

To manifest these arguments, we carry out our calculations, using the following reference quantities

$$[\tilde{\rho}] = 3\, \rho_0, \ \ [\tilde{M}] = 10^{22} M_{\odot}, \ \ [\tilde{V}] = c.$$

These are used to non-dimensionalize the field equations. Based thereon the reference radius reads: $[\tilde{r}] = [(3/4\pi)([\tilde{M}]/\tilde{\rho})^{1/3}] \approx 1.21$ AU. which yields $[\tilde{\tau}] \approx 10$ min.

Although the inward propagational speed, V_f, of the hadronization front, $\mathcal{F}^{HD}$, should be taken as an input parameter, we simply set V_f to be equal to the speed of light. The reason is that inside incompressible SuSu-matter with $\nabla P = 0$, communications are

11

conducted with the speed of light only.

Hence, the hadronization front would reach the center roughly after 10 minutes, whilst the expansion front, $\mathcal{F}^{EX}$, should have reached $r = 2 \times [\tilde{r}]$.

The production rate of normal matter $\dot{M}^{nor}$ and the corresponding total mass M^{nor} at $time = t$ read:

$$\dot{M}^{nor} = F_0 \left[1 + \left(\frac{tV_f}{r_0}\right)^2 - 2\left(\frac{tV_f}{r_0}\right)\right]$$
$$M^{nor} = M_0 \left[3\left(\frac{tV_f}{r_0}\right) - 3\left(\frac{tV_f}{r_0}\right)^2 + \left(\frac{tV_f}{r_0}\right)^3\right] \quad (38)$$

where $M_0 = (4\pi/3)\rho_{cr}r_0^3$ and $F_0 = (4\pi r_0^2) \times (\rho_{cr}V_f)$ are the reference total initial mass of the progenitor and the initial outward-oriented flux of energy, respectively.

In Fig. (3) we show the time-evolution of the spacetime topology during the propagation of the hadronization front without hydrodynamics. Here the mass of SuSu-fluid decreases whilst the mass of the newly created normal matter increases, thereby enforcing the spacetime to change its topology from flat into curved. On the other hand, the expansion front, $\mathcal{F}^{EX}$, which separates the enclosed curved spacetime from the unperturbed surrounding flat spacetime, starts propagating outwards at the speed of light.

When including hydrodynamics, the flow configuration mimics the classical relativistic shock tube problem (RSTP, see [24] for further details). In Fig. (4) the time-dependent motion of normal matter triggered by the pressure gradient under flat spacetime conditions is shown. Here, the matter is jettisoned into the surrounding flat spacetime with ultrarelativistic velocity, reaching very high Lorentz factors. In these calculations, the thermal energy is
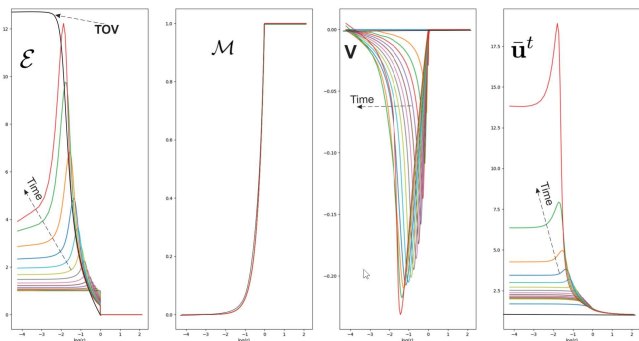
Figure 6: Snapshots of the radial distributions of the energy density $\mathcal{E}$, the total mass of normal matter, $\mathcal{M}$, the transport velocity $\mathbf{V}$ and the modified Lorentz factor $\overline{\Gamma}$ during the early stages of the contraction of the progenitor. In these calculations, the boundary conditions do not allow transport of normal matter into the surrounding. Obviously, the compressional front initially forms at the surface, starts propagating inwards. Depending on the EOS, the final configuration is a core in hydrostatic equilibrium whose interior is described by the modified TOV equation.

accounted for by modifying the total pressure as follows: $P_{tot} = P(\mathcal{E}) + P_{ram} = \mathcal{E} + \mathcal{E}V^2$, where P_{ram} stands for the ram pressure. Similar to the non-relativistic shock-tube problem, a rarefaction wave forms, which propagates in the opposite direction, expands the matter and lowers its pressure (first panel, Fig. 4).

In the following step, we allow spacetime to evolve according to Eq. (19). The initial configuration is a progenitor with incompressible SuSu-matter embedded in a flat spacetime. However, at $r = r_0$ boundary conditions were imposed, that prohibit escape of matter from the initial domain of the progenitor. Depending on the compactness parameter, $\kappa = r_0/r_S = \alpha_{bb}$ and the EOS, the surrounding
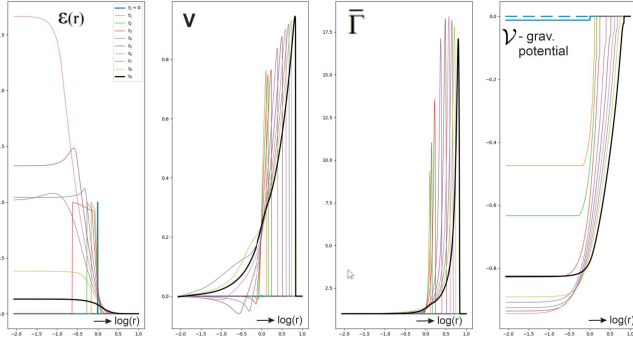
Figure 7: Snapshots of the radial distributions of the energy density $\mathcal{E}$, the transport velocity $\mathbf{V}$, the modified Lorentz factor $\overline{\Gamma}$ and the gravitational potential $\mathcal{V}$ for different times during the hadronization process of the progenitor and beyond, starting from $t_1 = 0$ (blue) and ending up at $t_9 = 6$ (black).

curved spacetime compresses the matter in the central region toward forming a hydrostatic core. Indeed, in the limit of $t \to \infty$ the equation for $\mathcal{V}$, which we term as the gravitational potential, converges to the TOV, which is usually used to model the interior of NSs in hydrostatic equilibrium (see Figs. 5 and 6). Whilst the matter accumulates in the very central region, the gravitational potential well becomes increasingly deeper.

When removing the BCs on the velocity and pressure at $r = r_0$, the resulting large pressure gradient jettisons the newly created hadrons into the surrounding spacetime with ultrarelativistic velocities, leaving little time for the matter to accumulate in the central region to form a core in hydrostatic equilibrium.

As anticipated, when the SuSu-matter in the outermost shell of the progenitor decays into hadrons, the surrounding spacetime starts curving. This, in turn, compresses the newly created normal matter via a compression front that follows, but is still slower than the inward-propagating hadronization front (see the first panel in Fig. 6). Had the compression front hit the center, then the infalling matter bounces back and turns into outflow (second panel in Fig.7). Note that the transport velocity increases with both time and distance from the center, and therefore is practically accelerating outwards relative to $\mathcal{O}_0$. In the third panel the modified Lorentz factor, $\overline{\Gamma}$ is displayed versus distance. We recall that:

$$
\overline{\Gamma}^2 = \begin{cases} \frac{g_{tt} + V^2 r_{rr}}{g_{tt} - V^2 r_{rr}} & : \text{General form} \\ 1 & : \text{Hydrostatic core embedded} \\ & \quad \text{in curved spacetime} \\ \frac{1 + \beta^2}{1 - \beta^2} & : \text{Flat spacetime.} \end{cases}
$$
(39)

Obviously, for matter configurations that are slowly contacting or in hydrostatic equilibrium, $\overline{\Gamma}^2$ is more indicative than the classical Lorentz factor. In the fourth panel the time-evolution of $\mathcal{V}$, which is dubbed gravitational potential, is displayed. Here, during the accumulation of matter in the central region, the gravitational potential becomes increasingly deeper, which agrees with the numerical experiment in Fig. (3). However, had the core entered the bouncing phase, which is expected to occur on the dynamical time scale, the spacetime at the background would start flattening, in accord with the minimum energy theorem (see Eq. [40] below). To clarify this point we note that in the stationary case, the minimum energy theorem states that the gravitational energy/mass, $\mathcal{E}_g$, of an object can be extracted from the curvature of the embedding

spacetime as follows:

$$\mathcal{E}_g = \frac{1}{16\pi} \lim_{r\to\infty} \int_{S^2} n^i g^{k\ell} \left(\frac{\partial}{\partial x^k} g_{\ell i} - \frac{\partial}{\partial x^i} g_{\ell k} \right) dS$$

$$= \begin{cases} 0 & \text{flat spacetime} \\ M_0 & \text{Schwarzschild spacetime.} \end{cases}$$

(40)

For further details see [26, 14].

In obtaining the last equality, we relied on the Birkhoff theorem, which states that the surrounding spacetime topology may be described by the Schwarzschild metric.

In the present time-dependent case, Birkhoff theorem is valid only in the domain between the shock front, $\mathcal{F}^{SH}$, and the expansion front $\mathcal{F}^{EX}$, only. Here the time-dependent gravitational potential reads:

$$\mathcal{V}(r,t) = \begin{cases} \mathcal{V}(r,t) & : r \leq r_{SH} \\ log\sqrt{1 - M_0/r} & : r_{SH}(t) \leq r \leq r_{EX}(t) \\ 0 & : r \geq r_{EX}(t), \end{cases}$$

(41)

where $r_{SH} \doteq V_{SH}\, t$, and $r_{EX} \doteq c\, t$ are the radial distances of both the shock and expansion fronts, respectively.

The integral may be transformed into an infinite series, where each summand represents the enclosed mass of a newly created ring of normal matter at a time t_n. Since the series converges to $\mathcal{M}_0$, the integral should be transformable into the sum of infinite discrete summands as follows:

$$\frac{1}{16\pi} \lim_{r\to\infty} \int_{S^2} (*) dS \xrightarrow[t=\frac{r}{c}\to\infty]{} \frac{1}{16\pi} \sum_{t_0=0}^{\infty} f(t_n) = \mathcal{M}_0,$$

(42)

where $f(t_n)$ corresponds to the time-dependent form of the integrand at time t_n. For $t \leq r_0/c$, the total

Figure 8: A schematic description of the evolution of spacetime (ST) topologies during the big bang event. Starting at the surface of the progenitor (BB), the hadronization front, $\mathcal{F}^{HA}$, starts propagating inwards with the speed of light, thereby converting the SuSu-matter into normal matter, and changing the topology of the embedding spacetime from flat into a curved one. The newly created normal matter is jettisoned in the direction of $-\nabla P$, thereby forming a shock-front $\mathcal{F}^{SH}$, which is then immediately overtaken by the outward-propagating expansion front $\mathcal{F}^{EX}$. The latter changes the spacetime topology from flat into a curved one. Relative to $\mathcal{O}_0$, both curved spacetimes between $\mathcal{F}^{HA}$ and $\mathcal{F}^{SH}$ (red colored) as well as between $\mathcal{F}^{SH}$ and $\mathcal{F}^{EX}$ (yellow colored) increase with time. However, as the total mass of normal matter is finite, the curved spacetime starts to flatten and converge to a flat on time scales much longer than the dynamical one, i.e. $\tau \gg \tau_{dyn}$.

14

mass of normal matter increases with time and the corresponding potential well becomes increasingly deeper.

For $t \geq r_0/c$ the total mass of normal matter enclosed within the outward-moving radius $r \geq r_{sh}(t)$ is $\mathcal{M}_0$, whereas the gravitational potential $\mathcal{V}(r,t) \sim log\sqrt{1 - \mathcal{M}_0/r_{EX}}$, and therefore decreases with time and distance. As a consequence, due to the significant increase of the volume enclosing the normal matter, the gravitational potential starts flattening in the inner part (see $\mathcal{V}$ in Fig. 7). In the limit of $\tau \gg \triangle\tau_0$, the curved spacetime would converge to a flat one and our observer $\mathcal{H}_0$ would hardly see anything, but a flat spacetime.

A comoving observer sitting at the shock front would experience deceleration if the expansion front is much faster than the shock front, whereas a stationary observer at the center would see the shock front accelerating outwards.

5   Summary and discussion

Based on our previous studies of glitching pulsars, an alternative model for the BB has been presented. Accordingly, pulsars are born with embryonic cores that are made of incompressible SuSu-matter. As pulsars evolve over cosmic times, these embryonic cores grow in mass and dimension to finally metamorphose into invisible dark energy objects. This phase corresponds to the lowest quantum energy state. According to our conjecture, the spacetime embedding SuSu-matter must be flat.

For $\tau \geq \tau_{14}$ these DEOs should have ample time to conglomerate into a cluster, then subsequently merge to form the $10^{20} M_\odot$ massive progenitor of the BB with a flat spacetime at the background.

At $t = 0^+$ with respect to $\mathcal{O}_0$, the progenitor underwent an abrupt decay, thereby initiating four fronts that started propagating in different directions and speeds (see Fig. 8):

- A hadronization front, $\mathcal{F}^{HA}$, that formed at the surface and propagated inward at the speed of light, behind which SuSu-matter was converted into virially hot and dissipative normal matter, which, in turn, interacted with spacetime and converted it into a curved one.

- An expansion front, $\mathcal{F}^{EX}$, of spacetime, which formed at the surface and propagated outwards at the speed of light, thereby changing the topology of spacetime from flat into a curved one.

- $\mathcal{F}^{HA}$ would be followed by the compression front $\mathcal{F}^{COM}$, which the surrounding curved spacetime exerts on the enclosed normal matter, but not on the incompressible SuSu-matter. Due to the opposing force of the pressure, $\mathcal{F}^{COM}$ would propagate much more slowly than $\mathcal{F}^{HA}$.

- Triggered by the gradient of the pressure of normal matter at the surface of the progenitor, a shock front, $\mathcal{F}^{SH}$, started propagating outwards, whose speed is determined by both the
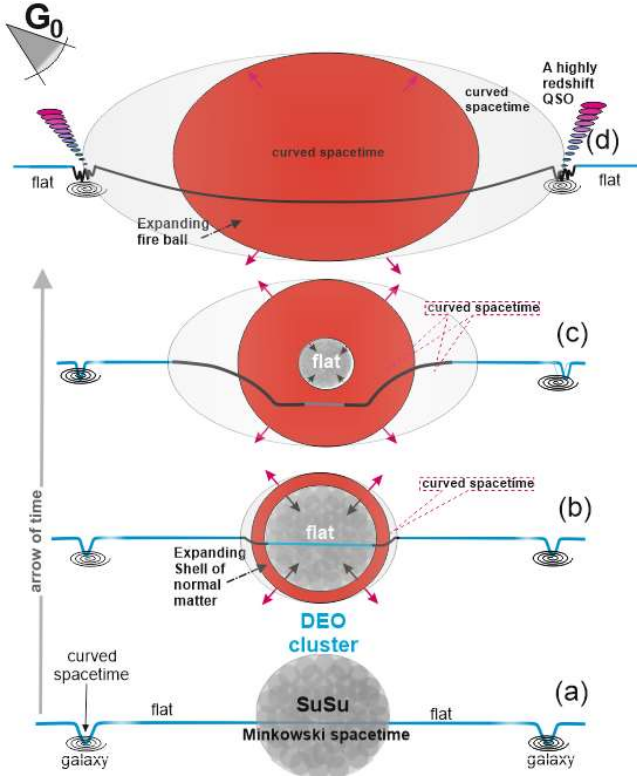
Figure 9: A schematic description of the BB-scenario as seen by the supra-observer $\mathbf{G}_0$: on time scales comparable to or even larger than the age of the universe, a certain number of DEOs find their ways to conglomerate and form a tight cluster, where they subsequently merge smoothly and form the hypermassive progenitor of the BB. At a certain time, it undergoes an abrupt decay, triggering a hadronization front, $\mathcal{F}^{HA}$, which starts propagating from outside-to-inside, thereby converting the SuSu-matter into normal dissipative matter and changing the spacetime topology from flat into a curved one. At the same time, the decay triggers an expansion front $\mathcal{F}^{EX}$, which starts propagating outwards, thereby changing the topology of the surrounding matter-free spacetime from flat into a curved one. Once $\mathcal{F}^{EX}$ has hit and marched throughout old and quiet galaxies, it sets them in active mode, which we identify as high redshift QSOs. For $\tau \gg \tau_{dyn}$ the curvature of spacetime embedding the BB-explosion starts flattening in accordance with the minimum energy theorem.

EOS and the ratio of the pressure across the surface. Given the perfect spherical symmetry of the progenitor and that $\mathcal{E} = P = 0$ in the surrounding flat spacetime, $\mathcal{F}^{SH}$ of the normal matter in the outermost shell would hardly differ from, though more slowly than $\mathcal{F}^{EX}$. This implies that the matter-free domain which is bounded between $\mathcal{F}^{SH}$ and $\mathcal{F}^{EX}$, increases with time. However, the outward propagational speed of the matter in the following shells must be smaller, as the corresponding matter still has to climb up the gravitational well in which it is located. For the stationary observer $\mathcal{H}_0$, this matter appears accelerating outwards, rendering its re-collapse into a BH.

In this paper, we have presented also the theoretical foundation of the scenario, by deriving the time-dependent GR field equations in combination with the general relativistic hydrodynamical equations.

A new metric, which unifies the Minkowski, Schwarzschild and Friedmann metrics has been presented and implemented in the present model of the BB. Moreover, a modified TOV-equation for modeling contracting relativistic objects has been presented.

A highly robust time-implicit numerical solver, which relies on preconditioning techniques within the framework of Krylov subspace iterative methods has been employed to solve the above-mention set of equations numerically.

The numerical results obtained are in line with the here-presented scenario. In Figs. (9 and 10) we

schematically outline the different aspects of the scenario, but the main consequences may be read as follows, though theoretical investigations and observational data are still needed to ensure their validities further:

- We conjectured that the spacetime inside zero-temperature QG-condensates that are motionless relative to remote stationary observers ought to be flat. This corresponds to the lowest quantum energy state, which should be compatible with the surrounding vacuum states [15, 16]. Putting a certain number of such QG-condensates, each component would be transparent to the other, and so they ought to overlap towards forming a parent condensate, whose mass and dimension are the linear addition of those of the individuals. The matter in the cores of massive NSs is expected most to share these properties, and therefore the spacetime embedding these cores should be flat. We note that the flatness requirement of spacetime inside zero-temperature QG-condensates is equivalent to demanding them to be in an incompressible state.

- Another implication of the above-mentioned conjecture is that the laws of nature would permit the existence of a universal maximum energy-density, ρ_{max}^{uni}, beyond which matter becomes purely incompressible. In this case, the matter is well-prepared to resist all types of external destructive perturbations, as communications are maintained at the speed of light.
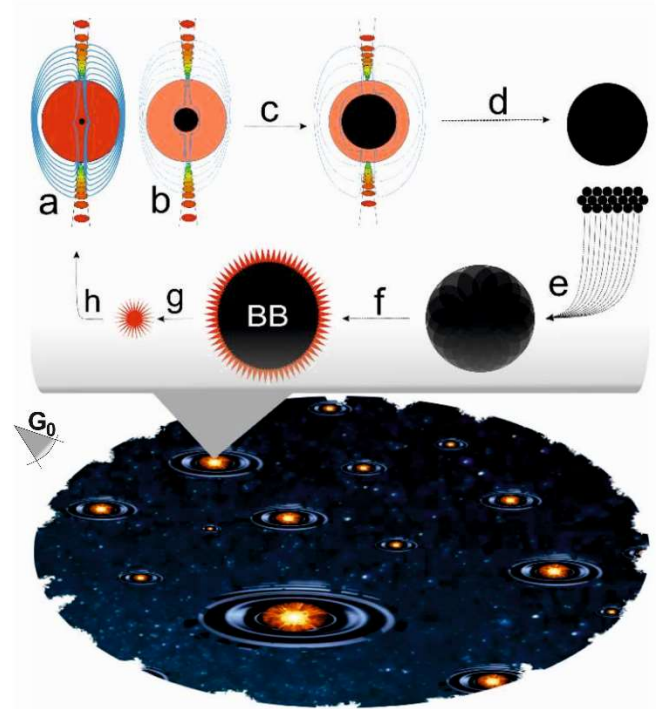

Figure 10: A schematic description of BB-cycles in the multiverse scenario as seen by the supra-observer $\mathbf{G}_0$. Pulsars are born with embryonic cores of incompressible SuSu-matter (a), these cores grow in mass and dimension in a discrete manner (b, c) and finally metamorphose the entire dead NSs into invisible DEOs (d). On time scales comparable to or longer than the age of the universe, part of these objects conglomerate to form a cluster of DEOs (e), that subsequently merge to form a hypermassive DEO (f), which serves as the progenitor of the next BB. At a certain time, it undergoes an abrupt decay (f), thereby hadronizing the entire progenitor and giving rise to a BB-explosion (f), later on the jettisoned matter cools down and forms stars, part of which collapse to form the next generation of pulsars.

In an infinite universe, these BB-cycles may occur in the sub-domains sequentially and/or in parallel as depicted in the lower panel.

17

Consequently, the collapse of astrophysical objects with incompressible SuSu-cores need not end up forming BHs, but the SuSu-cores would enforce the infalling matter to bounce off, through which they increase in masses and size.

Indeed, based on the numerical solution of the Gross-Pitaevskii equation for modeling Boss-Einstein condensates (see Sec. 2.4 in [14]), it was shown that the merger of two DEOs proceeds rather stably and smoothly, without developing destructive perturbations. This in turn may indicate that the NS-merger GW170817 may have formed a NS with a much more massive core, rather than collapsing into a stellar BH (see [27, 28, 29] for further details).

It should be noted here that the event horizon of a $10^{22} M_\odot$ massive object made of normal matter is of order 10^{27} cm. Hence, without invoking inflation and violating causality, our universe must theoretically have collapsed into a hypermassive BH. In the here-presented scenario, however, our universe is shown to expand forever, without invoking inflation and dark energy, whilst still respecting causality.

- The ADM mass is generally calculated from the integral (40), provided that the concerned object is standing there forever. However, in the time-dependent case, the causality condition requires the curved spacetime from which gravitational mass-energy is extracted, to have a finite

dimension. Recalling that the convergence of SuSu-matter into normal matter was completed after 10 minutes, generating a fireball with a fixed mass of $10^{22} M_\odot$, which must remain constant. As both the fireball and the embedding spacetime are expanding, the curvature must start flattening from inside-to-outside (see Fig. 7). In this case, the following two logical consequences emerge:

1. Once the outward-propagating expansion front, $\mathcal{F}^{EX}$, has hit and marched through faint and quiet galaxies, the local spacetime is perturbed and their contents must re-arrange their trajectories, thereby transforming the galaxies into active modes, that we observe today as active galaxies and powerful QSOs.

2. After the first 10 min, the total mass of normal matter was $10^{22} M_\odot$, and was enclosed inside a sphere of radius 2.4 AU. Since then the curvature of spacetime has been continuously flattening, which yields a relative curvature: $Q(t = today)/Q(t = 10\,\text{min}) \sim [r(t = 10\,\text{min})/r(t = today)]^2/ \approx 10^{-30}$. This implies that the universe today must be extraordinarily flat.

- Based on the here-presented scenario, we conclude that BB-explosions are local recurrence phenomena in an infinite universe, that may take off from time to time in different subdomains sequentially and in parallel. These

sub-domains are dynamical; they may overlap with others, disappear, or even be created anew. Each sub-domain may be populated by all types of objects and its dimension and age are determined by the time it takes to restore the spacetime topology into a flat one. The life-cycle of each sub-spacetime follows the same evolutionary scenario of the BB in our universe: here pulsars evolve into NSs, these become DEOs. A number of DEOs may conglomerate in a certain location in the sub-domain, they merge and form a giant progenitor made of SuSu-matter. The progenitor undergoes an abrupt decay that leads to its entire hadronization, thereby creating a giant fireball. Its content cools down and stars are formed, part of which collapse to form pulsars and so on.

- The total mass of normal matter-made objects that evolved from the BB of our universe may most likely be much lower than expected, as spacetime surrounding the progenitor of the BB may have been populated by numerous dead objects and galaxies.

- SuSu-matter can be found in pulsars, NSs, magnetars and even in stellar and supermassive BH-candidates. This implies that these objects may be much more massive than predicted from observing normal and luminous matter. This is a direct consequence of the flat spacetime topology that embeds SuSu-matter.

References

[1] Bromm V., (2013), astro-ph/arXiv:1305.5178

[2] Laporte N., Meyer R.A., Ellis R.S., et al., (2021), MNRAS, 505, 3

[3] Diehl R., Halloin H., Kretschmer K., et al., (2006), Nature, 439, 45

[4] Sartore N., Ripamonti E., Treves A., Turolla R., (2010), A&A, 510, A23

[5] Fan, X., Wang, F., Jinyi Yang, J., et al. (2019), ApJL, 870, L11

[6] Oesch, P. A. et al. (2016), Astrophys. J. 819, 129

[7] Espinoza, C.M., Lyne, A.G., Stappers, B.W. and Kramer, C. (2011) MNRAS, 414, 1679

[8] Roy, J., Yashwant Gupta, Y. and Lewandowski, W. (2012) MNRAS, 424, 2213

[9] Hujeirat, A.A., (2018), Journal of Modern Physics, Vol.9, No. 554

[10] Hujeirat, A.A., Samtaney R., (2019), Journal of Modern Physics, Vol.10, No. 1696

[11] Ashton, G., Lasky, P.D., Graber, V. and Palfreyman, J.,(2019), Astro-ph. 1907.01124

[12] Hujeirat, A.A., (2020), Journal of Modern Physics, Vol.11, No.11

[13] Glendenning, N.K., (2007), Special and General Relativity, Springer

[14] Hujeirat, A.A., (2021), Journal of Modern Physics, Vol.12, 937

[15] Lee, T.D., (1979), Lecture at Columbia University, Preprint CU-TP-170

[16] Donoghue, J.F. , (1980), Phys. Rev. D, 22, 7

[17] Shuryak, E.V., (2004), arXiv: 0405066v

[18] Pasechnik, R., Šumbera, M., (2017), arXiv:1611.01533v3

[19] Guth, A.H., (1981), Physical Review D, 23, 347

[20] Linde, A.D., (1982), Physics Letters B, 108, 389 doi:10.1016/0370-2693(82)91219-9

[21] Steinhardt, P.J., Phys. Rev. Lett., 48, 1220

[22] Valerio Bozza, V., (2022), in BouncingCosmologies, 8, 37

[23] Hobson, M.P., Efstathiou, G. & Lasenby, A.N., (2015), CUP

[24] Fischer, M.S., & Hujeirat, A.A., (2020), arXiv.200412310

[25] Hujeirat, A.A., Thielemann, F-K., (2009), Inf.Springer, 32, 496

[26] Witten, E., (1981), Commun. Math. Phys. 80, 381

[27] Abbott et al., Ligo & Virgo Collaboration, (2017), ApJL, 848, L12

[28] Piro L., Troja E., Zhang B., (2019), MNRAS, 483, 1912

[29] Hujeirat, A.A., Samtaney, R., (2020), Journal of Modern Physics, 11, 11